# Direct sensing of superoxide and its relatives reactive oxygen and nitrogen species in phosphate buffers during cold atmospheric plasmas exposures

# Direct Sensing of Superoxide and its Relatives Reactive Oxygen and Nitrogen Species in Phosphate Buffers during Cold Atmospheric Plasmas Exposures

Fanny Girard-Sahun[a,b], Pauline Lefrancois[b], Vasilica Badets[b], Stéphane Arbault[*b, c], Franck Clement[*a]

[a] *Université de Pau et des Pays de l'Adour, E2S UPPA, CNRS, IPREM UMR 5254, 64600 Anglet, France.*

[b] *Univ. Bordeaux, CNRS, Bordeaux INP, ISM, UMR 5255, NSysA group, F-33402 Talence, France.*

[c] *Univ. Bordeaux, CNRS, Bordeaux INP, CBMN, UMR 5248, MSB group, F-33600 Pessac, France.*

[*] Corresponding authors : stephane.arbault@u-bordeaux.fr, franck.clement@univ-pau.fr

**ABSTRACT:** This study aims at sensing *in situ* some Reactive Oxygen and Nitrogen Species (RONS) and specifically superoxide anion ($O_2^{\bullet-}$) in aqueous buffer solutions exposed to Cold Atmospheric Plasmas (CAPs). CAPs were generated by ionizing He gas shielded with variable $N_2$ / $O_2$ mixtures. Thanks to ultramicroelectrodes protected against the high electric fields transported by the ionization waves of CAPs, the production of superoxide and several RONS was electrochemically directly detected in liquids during their plasma exposure. Complementarily, Optical Emissive Spectroscopy (OES) was used to study the plasma phase composition and its correlation with the chemistry in the exposed liquid. The specific production of $O_2^{\bullet-}$, a biologically reactive redox species , was analyzed by Cyclic Voltammetry (CV), in both alkaline (pH 11), where the species is fairly stable, and physiological (pH 7.4) conditions, where it is unstable. To understand its generation with respect to the plasma chemistry, we varied the shielding gas composition of CAPs to directly impact on the RONS composition at the plasma-liquid interface. We observed that the production and accumulation of RONS in liquids, including $O_2^{\bullet-}$ , depends on the plasma composition, with $N_2$-based shieldings providing the highest superoxide concentrations (few tens of micromolar at most) and of its derivatives (hundreds of micromolar). *In situ* spectroscopic and electrochemical analyses provide a high resolution kinetic and quantitative understanding of the interactions between CAPs and physiological solutions for biomedical applications.

## INTRODUCTION

Reactive Oxygen and Nitrogen species (ROS, RNS, commonly merged into RONS) are involved at multiple levels of aerobic biological processes in both physiological and pathological situations.[1,2] These small and unstable molecules (particularly free radicals such as $HO^{\bullet}$, $O_2^{\bullet-}$, $NO^{\bullet}$ or $NO_2^{\bullet}$) are able to modify redox-sensitive signaling pathways, to modulate cellular functions, as well as to induce damages to cell components and eventually cell death.[3–6] The modulation of RONS quantities and ratios in cells and tissues is necessary to determine what precise mechanisms are involved during cellular modifications, in order to possibly control or inhibit the occurring processes.

Cold atmospheric plasmas (CAPs) have gained in interest over the last decade because these physico-chemical processes are able to produce diverse types and modulated quantities of RONS. CAPs are partially ionized gases composed of a reactive gaseous mixture and different energy components: electrical charges (electrons and ions) inducing local high electric fields, excited atoms and molecules emitting photons in the UV-visible range, local thermal effects. CAPs can be generated at room temperature and at atmospheric pressure which allows potent biological and biochemical applications. Due to the chemical reactivity of the gas phase, CAPs thus yield large amounts and complex mixtures of chemical species. When interacting with solids, liquids or gases, their chemical reactivity is modified and allows numerous applications. Wound healing and skin regeneration seem thus to be promoted by local applications of plasmas, as shown in various works.[7–9] Other works are developed in cancerology showing interesting aspects of CAPs against tumors and cancer cells.[4,5,10,11] Applications are also demonstrated in sterilization and decontamination with positive effects against germs (bacteria, fungi, viruses).[12–15] The effects on plasma-treated cells and tissues are often described in the literature to be mainly due to RONS, inducing biological modifications, such as membrane permeability increase, DNA breaking, mitochondrial uncoupling, antioxidant responses, etc.[4,5,10] It is important to note that the different plasma energy components (RONS, charges, electric fields, photons, local thermal effects) will play a more or less important role on the expected biological effects. Results observed are depending on how CAPs are applied to a sample (directly or in remote conditions, by controlling the air environment and its humidity around sample or not).[16–19] The features of the sample (dimensions, composition, conductivity, etc.) are also influential on the observed effects as well as on the plasma processes.[20–24] Local electric fields are also believed to have a synergetic effect with RONS produced by plasmas.[20–23]

To date, the exact mechanisms of RONS production in the gas phase and propagation into liquids, cells or tissues, as well as their action mechanisms remain partially understood. It is particularly challenging to analyze free radicals in gases or liquids due to their short lifetimes. Most of the current detection methods are based on optical analyses of the gas phase and on

indirect detections in solution via various kinds of molecular probes: spin traps (EPR spectroscopy), chemical (reagents, scavengers) or fluorescent probes (spectrophotometry).[25–28] In this last case, measurements are not performed during the medium exposure to plasma. Instead, the liquid sample is collected after exposure and mixed with the probe but the short lifetimes of RONS impairs the measurement accuracy. In addition, if the probe is added during the sample exposure, a potential chemical interaction with the plasma is expected, inducing false positive or negative responses. Even if information about the long-lived RONS generation by CAPs in liquids have thus been obtained, it is necessary to decipher on the dynamics of the plasma-induced chemistry in liquids. However, some major difficulties remain that we propose to tackle in this work: 1/ to detect *in situ* some unstable RONS in liquids exposed to plasmas; 2/ to study the dynamics of RONS production and evolution (reactions, decomposition, etc.) in the liquid during and after its exposure; 3/ to draw correlations between the plasma phase and the liquid chemistries, which is an essential point to understand the induced phenomena.

For this study, we used an electrochemical approach to detect in direct mode and *in situ* the production of RONS in liquids during their exposure to plasmas.[29] This setup is based on a shielded and grounded three-electrode setup composed of an ultramicroelectrode (UME), used as working electrode, a reference electrode and a counter electrode, all being efficiently protected from the electromagnetic environment of the plasma setup.[29] Consequently, this setup allows to perform electrochemical analyses in solution during the plasma experiment without any additional sampling protocol or revealing probes. Thus, we reported the measurement in a phosphate buffer saline solution (PBS pH 7.4) of the production of two major long-lived RONS: hydrogen peroxide ($H_2O_2$) and nitrite anion ($NO_2^-$)) under a plasma exposure generated with high electric fields, up to 10-20 kV.cm$^{-1}$.[30,31] A recent work from Wende et al. has demonstrated complementary results with another electrochemical set-up.[32]

The goal of such an *in situ* and direct electrochemical detection is to monitor short-lived species and in particular the superoxide radical anion $O_2^{\bullet-}$. This free radical is important in biological oxidative stress processes[33]. Though this is not a good oxidant by itself, it can react with membrane phospholipids, DNA bases, enzyme hems (Fe-S clusters) and further lead to stronger ROS and RNS oxidants ($H_2O_2$, $HO^\bullet$, $HO_2^\bullet$, $ONOO^-$…). Superoxide is involved in various gas and liquid phase reactions of the CAPs. In the gaseous phase $O_2^{\bullet-}$ can be produced by electronegative attachment with electronic collisions following the reaction:

$$O_{2\,(gas)} + e^- \rightarrow O_{2\,(gas)}^{\bullet-} \quad (1)$$

In the liquid phase, $O_2^{\bullet-}$ is the mother species of $H_2O_2$ and $O_2$ by disproportionation in physiological conditions according to the following reaction:

$$2O_2^{\bullet-} + 2H^+ \rightarrow H_2O_2 + O_2 \quad (2)$$

Superoxide is also known to react with $H_2O_2$ in the Haber-Weiss reaction, catalyzed by metal ions, following the reaction:

$$O_2^{\bullet-} + H_2O_2 \xrightarrow{M^{(n+1)+}/M^{n+}} HO^\bullet + HO^- + O_2 \quad (3)$$

In addition, $O_2^{\bullet-}$ favorably reacts with nitric oxide $NO^\bullet$, to produce the peroxynitrite anion $ONOO^-$ species following the reaction:

$$NO^\bullet + O_2^{\bullet-} \rightarrow ONOO^- \quad (4)$$

These diverse reactions involve and lead to other RONS, as was highlighted in multiple studies about plasma-treated water, aqueous buffers or media.[1,2,34,35] In particular, we showed the presence and quantified the peroxynitrite anion $ONOO^-$ in alkaline buffers exposed to He-CAPs in air.[19,36] This result suggests the prior existence of both $NO^\bullet$ and $O_2^{\bullet-}$ in the gas and/or liquid phases. Indeed, $NO^\bullet$ was identified as a major emissive species in the gas phase as shown by our team.[19,37] The present work thus aims at proving the transient existence of $O_2^{\bullet-}$ in plasma-treated solutions by detecting its electrochemical signature and quantifying its fluxes. Superoxide was previously reported as a key species in studies of CAP-treated water or buffers, but only based on indirect detection methods and dyes including EPR, chemiluminescence and fluorescence [16,38–40]. Superoxide concentrations accumulated in aqueous solutions at physiological pH were estimated as a few micromolar. However, as explained above, these methods usually raise analytical concerns about their selectivity (differentiation between ROS), preparation methodology and about their kinetic and quantitative resolutions. Contrarily, in the present work, we performed a direct electrochemical detection of superoxide anion at selective ultramicroelectrodes in solutions exposed to CAPs. Alkaline and physiological pH conditions were used to modulate the superoxide anion chemical stability. Finally, under modulation of the CAP shielding gas environment, we established correlations between the gaseous chemical composition and the nature of biologically-active RONS including $O_2^{\bullet-}$ delivered in CAP-exposed solutions.

## EXPERIMENTAL SECTION

**Reagents**. PBS was from PAN BIOTECH (pH 7.4, KCl 0.003 mol.L$^{-1}$; $KH_2PO_4$ 0.002 mol.L$^{-1}$; NaCl 0.137 mol.L$^{-1}$; $Na_2HPO_4$ 0.01 mol.L$^{-1}$, no $Mg^{2+}$ nor $Ca^{2+}$). Solutions of $H_2O_2$ and $NaNO_2$ were from Sigma Aldrich (France). Alkaline PBS (pH 11) was obtained by successive addition of NaOH (Sigma Aldrich) in PBS (initial pH 7.4).

**Plasma setup**. Figure 1 shows two detailed schemes (Figure 1A and 1B) and a photography (Figure 1C) of the experimental setup used for this study and previously described.[19] It consists in the generation of an ionization wave propagating in a quartz tube included in another larger quartz tube thus allowing to control the gaseous environment (called shielding gas) around the plasma phase (called carrier gas).[18,19,41,42] Herein, the carrier gas is helium and is referred also to as working gas. Its partial ionization is obtained from pulsed high voltages applied between specific electrodes arranged in a Dielectric Barrier Discharge (DBD) configuration. This ionization leads to the ionization of the shielding gas used, thus forming the so-called CAPs. Three compositions of shielding gas were used, which depicted clear differences in the induced chemistry, both in the gas and liquid phases : 100 % $N_2$, 80 % $N_2$-20 % $O_2$ and 100 % $O_2$.[19] Gas flow rates were set as following: 1.67 slm for the helium working gas (purity 99.999%) and 0.03 slm rate for the shielding gas ($N_2$, $O_2$ 99.9995 % from Linde), for a total gas flow of 1.7 slm. Adequate mass flow controllers connected to a flow-bus were used for helium (EL-FLOW, Bronkhorst High-Tech) as well for $O_2/N_2$ mixtures. The electrical parameters are : High Voltage positive pulses of 7.5 kV in amplitude, 1 µs in duration, 10 kHz repetition frequency and 1% duty cycle.[19]

**Plasma treatment of physiological and alkaline buffer solutions**. 6 mL of PBS (pH 7.4 or 11) solutions were exposed to plasmas in a homemade quartz cuvette (dimensions: external diameter 44 mm, inner diameter 41 mm, depth 40 mm) as previously described.[29] We kept constant a 20 mm-distance between the end tube of the plasma device and the solution (see characteristic distance "a" in Figure 1), as well as a distance of 7±1 mm between the tube wall and the cuvette (characteristic distance "b" on Figure 1). Also, the cuvette was placed over a metallic support connected to the ground in order to ensure a constant potential to the sample.

**Optical emissive spectroscopy (OES)**. The chemical composition of the gas phase was analyzed by optical emissive spectroscopy. A wideband optical fiber (Ceramoptec UV 1500/1590 N) equipped with a diaphragm was placed at 12 ± 1 mm (characteristic distance "c" on Figure 1) from the plasma stream, and closest to the liquid surface (4 ± 1 mm, characteristic distance "d" on Figure 1). The wavelength-integrated light was then probed by UV-NIR OES between 200 and 900 nm where the emitted light was focused on the grating of a high-resolution spectrometer (1000M Jobin Yvon, 1200 groves.mm$^{-1}$, maximum spectral efficiency at 500nm) equipped with a CCD 3000 V light detector. During plasma exposure of PBS solutions, the emissive intensity of the following excited species was recorded over time during at least 30 minutes: $N_2^+$ (First Negative System FNS) at 391 nm, the second order of HO$^\bullet$ at 618 nm, $N_2$ (First Positive System FPS) at 762 nm and O at 777 nm. However, considering the bandwidth of our optical system it was not possible to detect some low emissive species such as nitric oxide NO$^\bullet$. The acquisition time was adapted to each species and the first spectrum was recorded 2.5 minute after the plasma was turned ON, after baseline stabilization in the PBS solution.

**Electrochemical in situ experiments.** We technically reported previously the possibility to perform *in situ* electrochemistry in a solution during its plasma exposure.[29] The main difficulty associated with such experiments is to apply low potential differences (mV) and measure low current variations (below nA) at the WE (potentiostat BioLogic, VSP-300 equipped with low current modules) when the solution is simultaneously exposed to very high electric fields (several 10 kV.cm$^{-1}$) imposed by CAPs. Measurements were realized using a three-electrode electrochemical configuration shielded from the electric environment : two grounded containers (a glass capillary covered by an aluminum foil connected to the ground via a cable and two layers of insulating shafts) were used (Figures 1B, 1C): the first contained the working ultramicroelectrode (WE; two UME could be inserted to perform simultaneous cyclic voltammetry and chronoamperometry or to have duplicates) and an Ag-AgCl reference electrode (REF; Ag wire anodized in NaCl 1M to obtain a stable AgCl deposit on its surface), separated by only few mm-distance within the capillary; the second contained the counter-electrode (CE), separated from the WE in order to prevent from chemical interferences between both (Figure 1B). The distance between the containers and the plasma impact point was searched to be minimum, i.e. to do measurements close from the source, without leading to any connection between the electrodes and the ionization wave in the solution. This is indeed mandatory that the electrochemical setup would not become the ground for the plasma in solution, such situation would be harmful for the potentiostat. Then, the distance between containers and plasma impact point was kept at ≈ 20 mm (characteristic distance "e" in Figure 1A). To detect RONS generated in PBS during plasma exposure, cyclic voltammograms were achieved between -0.2 V and +0.5 V vs. Ag/AgCl or between -0.1 V and +0.9 V, at 20 mV.s$^{-1}$ scan rate.[19,36] For more clarity, only the forward part of all voltammograms is depicted in all Figures. Moreover, stirring of the solution during experiments was necessary to improve mass transport of the produced species from the plasma impact point in the PBS toward the WE surface.

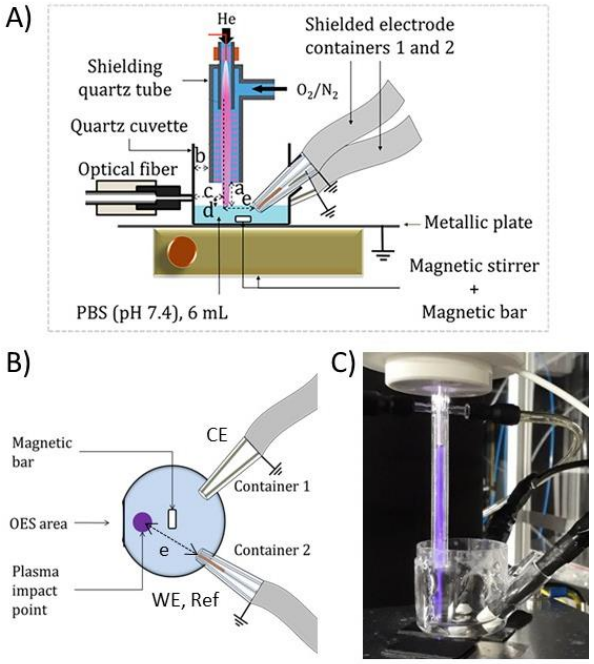


**Figure 1.** Scheme from profile (A) and top view (B) (not at scale), plus photography (C) of the experimental setup developed in the study. The setup includes: the plasma source, a device providing a surrounding gaseous environment, an optical fiber for the analysis of the gas phase by OES, the cuvette containing the solution to be exposed (6 mL of PBS) and two shielded containers incorporating 2 counter electrodes in the container 1, and 2 working ultramicroelectrodes together with the reference electrode (Ag/AgCl) in the container 2. Characteristic distances of the setup described in A) are: a = 20 mm; b = 7±1 mm; c = 12±1 mm; d = 4±1 mm; e = ~20 mm.

## RESULTS AND DISCUSSION

OES analysis of the plasma phase during the exposure of PBS solutions

In a previous work, we studied the gas phase chemistry of CAPs produced in shielded gaseous environments.[19] Shielded CAPs thus produced (with helium as the energy carrier gas) were analyzed by using Optical Emission Spectroscopy (OES) and by varying the gaseous environment (three typical $O_2/N_2$ ratios). This analysis gives a good assessment of some excited species generated in the gas phase that eventually produce RONS in the liquid phase. However, it would be of interest to decipher better on the chemistry at the gas/liquid interface, since this is the location where is determined the fate of chemical species in the liquid phase. In this study, we sought to analyze the emissive excited species as close as experimentally possible to the liquid surface, i.e., at d ≈ 4 mm distance based on the dimensions of the sensing optical fiber and setup for its positioning (see Figure 1 and paragraph 4 - experimental section).

In order to implement the electrochemical sensors in the cuvette, we used an open configuration. In this configuration

(Figure 1A) the ionization wave propagates over 20 mm in air before reaching the liquid (Figure 1). To verify if the benefit of the gaseous shielding setup remained, we varied the shielding gas composition and recorded the intensity of various gaseous molecular excited species (see details in the experimental section and emission spectra in Figure S1 of SI). $HO^{\bullet}$ molecules are expected to combine in the gas phase or at the gas-liquid interface, to produce $H_2O_2$, which was previously quantified in plasma-exposed PBS solutions for various $O_2/N_2$ ratios.[19] The $H_2O_2$ concentration was directly correlated to the $HO^{\bullet}$ amount in the gas phase, with a maximum value for 100% $N_2$ flow of shielding gas. Consequently, we first measured here the variation of $HO^{\bullet}$ molecule intensity by OES for various shielding gas compositions in parallel with the electrochemical analyses. Shielding gas compositions were chosen as variations of an aerobic condition, i.e. one mimicking a pure air (80% $N_2$-20% $O_2$) and two composed of each individual gas (100% $N_2$ or 100% $O_2$). The maximum emission intensity at 618 nm corresponding to the second order of the excited hydroxyl molecule was normalized and plotted as a function of time for each condition (see Figure 2A). Similarly, we followed other excited species such as $N_2^+$ (FNS: First Negative System) at 391 nm, $N_2$ (FPS: First Positive System) at 762 nm and O at 777 nm (see Figures 2B, C, D). The corresponding emissions clearly indicate that our plasma set-up allows to propagate electromagnetic ionization waves with enough energy for the production of excited species, the dissociation and the ionization of molecules. Among the species involved, excited and metastable state of helium $He(2^3S_1)$ with high energy level of 19,82 eV is of a great importance as it can carry sufficient energy in the gas.[43] Remember here that metastable are long-lived gaseous excited species which act as energy holder particles.[44] Due to numerous mechanisms, energy transfers with electronic collisions and excited species lead to specific other metastable or radiative excited states depending here of the shielding gas used. These metastable states are important because they are involved in energy transfer that produces RONS. By instance we can cite nitrogen metastable state $N_2(A^3\Sigma_u^+, 6.17\,eV)$ and singlet oxygen $O_2(a^1\Delta_g, 0.98\,eV)$ so noted in spectroscopic notation (or $^1O_2$ in chemistry), which are involved in the fate of $HO^{\bullet}$ and $O_2^{\bullet-}$ as suggested for instance in equations (5) to (7):[19,45]

$$N_2(A^3\Sigma_u^+) + H_2O \rightarrow HO^{\bullet} + H^{\bullet} + N_2 \quad (5)$$

$$O_2^{\bullet-} \rightarrow O_2(a^1\Delta_g) + e^- \quad (6)$$

$$O_2^{\bullet-} + HO^{\bullet} \rightarrow O_2(a^1\Delta_g) + OH^- \quad (7)$$

In Figure 2A it appears very clearly that the emissive intensity of $HO^{\bullet}$ depends on the shielding gas ratio: the intensity is maximum for 100 % $N_2$ (blue triangles), about 40 % lower for a ratio of 80 % $N_2$-20 % $O_2$ (green dots) and 80 % weaker for 100 % $O_2$ (red squares). These results are similar to the ones obtained in our closed-cell configuration, when plasma-liquid interactions are not influenced by ambient air.[19]

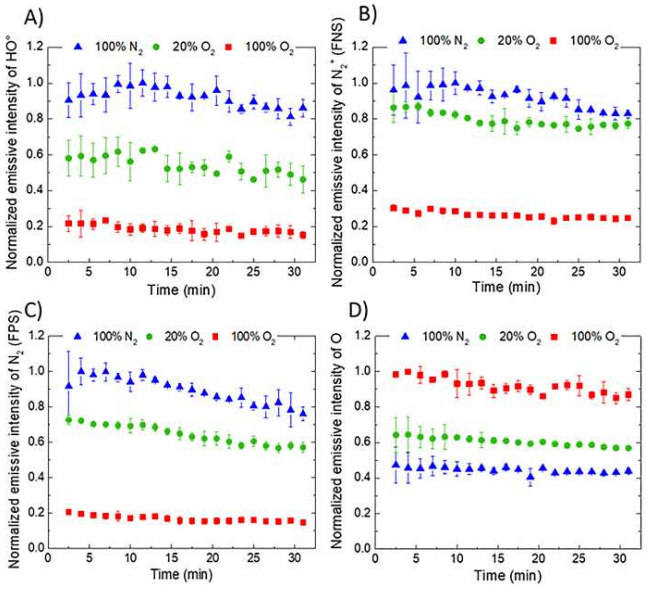


**Figure 2**. Normalized intensity of (A) $HO^{\bullet}$; (B) $N_2^+$ (FNS); (C) $N_2$ (FPS) and (D) O species measured by OES for 30 minutes during plasma exposure at the surface of a PBS solution (pH 7.4, 6 mL), for 100% $N_2$ (blue triangles), 80% $N_2$/20% $O_2$ (green dots) and 100% $O_2$ (red squares) shielding gases.

Thus, in a first assumption, we would expect higher $H_2O_2$ concentrations in the treated PBS for 100 % $N_2$ -shielded CAPs. For both $N_2^+$(FNS) and $N_2$ (FPS), the pure nitrogen shielding is logically the one giving the maximal intensities, followed by 80 % $N_2$-20 % $O_2$ and 100 % $O_2$ (Figure 2B and 2C). The trend is reverse for atomic oxygen (Figure 2D): 100 % $O_2$ is a more favorable shielding gas for O production. Moreover, in every case we observed a slight decrease of the intensity over time, 10 % at most. This phenomenon could be due to a weak evaporation process that was evidenced in a previous work.[36] We assume that this phenomenon can occur in these conditions as well, especially since the liquid is exposed for longer times (~30 min). Consequently, the level of the liquid surface may slightly diminish during CAP exposure, therefore increasing the characteristic distance *a* and decreasing the plasma impact point diameter. As a consequence, an evaporation process should induce a slight decrease of the emission intensities, as observed in Figure 2. Nevertheless, this first set of results shows that CAPs, whatever the composition of the shielding gas is, induce a continuous flow of reactive species at the interface between the gas and liquid phases. The chemistry of the liquid phase was then analyzed during and after its exposure to plasmas to establish correlations between the gas phase chemistry and some RONS appearing *in vitro*.

**Electrochemistry in solution under plasma exposure**

In our previous works, we first analyzed long-lived RONS such as $H_2O_2$, $NO_2^-$ and $NO_3^-$ produced by CAPs in PBS.[19,29,36] Peroxynitrite anion ($ONOO^-$), a short-lived RNS at physiological pH was also detected and quantified in PBS in alkaline conditions (PBS pH 12), where the anion is much more stable than at pH 7.4.[19,36] Some questions still remain about intermediate chemical reactions occurring during a plasma exposure of the liquid phase, the physiological buffer PBS pH 7.4 herein. In particular, short-lived species such as radicals are difficult to analyze though they must be considered in mechanistic studies. To do so, it is necessary to access to the fast chemistry occurring in solution. For this purpose, we used

a dedicated setup, whose development was reported previously,[29] and is based on an electrochemical detection with ultramicroelectrodes of soluble and electroactive RONS. Ultramicroelectrodes (UMEs) offer key analytical advantages related to their dimensions, including short-response times (reaching sub-millisecond values), low-volume sensing (nano to micro-liters), steady-state measurements of *in vitro* redox species and improved sensitivity (higher S/N ratio due to lower capacitances). One or two UMEs, as well as the reference and counter-electrodes, are inserted into electrically-shielded and grounded containers (glass capillary covered by several sheets of a conductive aluminum foil and electrically-insulating polymer sheets; see material and methods section) and are thus well protected from the surrounding strong electric field, i.e. the electromagnetic ionization wave transported by the plasma. The WE, i.e. the UME is placed with the REF electrode in one container to minimize their inter-distance while the CE electrode is placed in the second container to prevent from a chemical cross-talk with the WE in a confined volume. The distance between the plasma contact point at the solution (under constant stirring) and the shielded UMEs is 20 mm at most, leading to a quite fast detection (below 1 second) of the chemical variations due to RONS dissolution in solution and an improved sensitivity for low concentrations of these species (sub-micromolar range in chronoamperometry with platinized UMEs)[46,47].

The setup was previously shown to provide a direct monitoring of $H_2O_2$ and $NO_2^-$ production in solution under its plasma exposure.[29] Their kinetics of appearance and concentration rises were determined based on calibration curves with the same UMEs. Herein, the method was used to analyze a short-lived redox species, the superoxide anion $O_2^{\bullet-}$. The electrochemical signature of $O_2^{\bullet-}$ at platinized UMEs was recently characterized *in vitro* from a pure chemical source ($KO_2$ salt dissolved in PBS at different pHs).[48] A well-defined voltammetric redox wave for $O_2^{\bullet-}$ was detected (stable in alkaline PBS, pH 11-12), showing a maximum oxidative current, i.e. a plateau current, at 0 V vs Ag/AgCl. Based on this electrochemical study, we searched here for detecting $O_2^{\bullet-}$ in solutions during their plasma exposures, first at alkaline pH 11 to guaranty $O_2^{\bullet-}$ stability, and then at pH 7.4 in physiological conditions.

**Study at alkaline pH**

The accuracy of the *in situ* measurements was comparable during exposure and in absence of plasma thanks to the electrical shielding of the electrochemical cell, meaning that a precision of 1-2 mV on the potential applied to the UMEs was reached while a sub-nanoampere sensitivity for the detected amperometric currents was obtained. Besides, the voltammetric responses of long-lived species, i.e. $H_2O_2$ and $NO_2^-$, were characterized at different pHs and concentration ranges.[19,29] We performed a continuous detection by cyclic voltammetry in alkaline PBS, pH 11, exposed to CAPs. Cyclic Voltammograms (CVs) were recorded in a potential window, from -0.2 V to +0.5 V vs. Ag/AgCl, enabling to detect $H_2O_2$, $O_2$ and $O_2^{\bullet-}$ on platinized UMEs.[48] Note that voltammograms were continuously recorded in solution, during the plasma exposure and until the plasma was turned OFF in order to monitor the chemical evolution in solution.

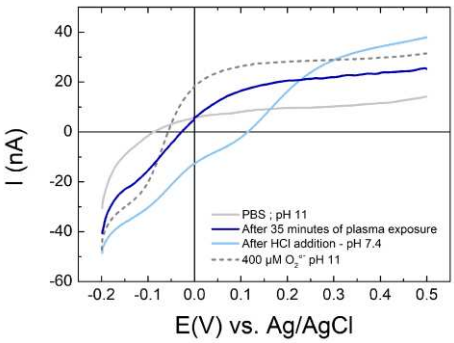


**Figure 3.** Cyclic voltammograms realized in PBS solution at pH 11 before (grey line) and after 35 min of plasma exposure (dark blue line, with shielding 100% $N_2$) compared with CV obtained in $O_2^{\bullet-}$ solution (400 µM, pH 11 grey dashed line) under magnetic stirring. After plasma exposure, addition of HCl changed pH from 11 to 7.4 (light blue line). Scan rate 20 $mV.s^{-1}$.

Results on Figure 3 compare the response of the starting PBS pH 11 solution with the one after 35 min of CAP exposure (100 % He, 100 % $N_2$ shielding gas), to the one of the CAP-treated solution but shifted in pH to reach a physiological level (pH 7.4) and to a reference voltammogram of a superoxide solution (chemically generated) in PBS pH 11. After about 35 minutes of plasma exposure (dark blue line), the CV depicts one clear reversible electrochemical wave, centered at -0.05 V vs Ag/AgCl. This reversible signal can be very likely attributed to superoxide anion, while the reductive current starting at more reductive potentials, i.e. at -0.15 V, corresponds to the $O_2$ reduction ($HO_2^-$ may also contribute though this species gives a poorly defined CV signal at alkaline pH).[48] The detection of $O_2^{\bullet-}$ was confirmed by comparing the response detected in the plasma-treated PBS with the one of a superoxide anion solution (from $KO_2$ salt solubilized in PBS) with Black-Pt UMEs (experiment performed independently; grey dashed line). In addition, this hypothesis was confirmed by shifting the pH value of the plasma-treated solution from 11 to 7.4 by additions of concentrated HCl (plasma was OFF). The pH change led to $O_2^{\bullet-}$ disproportionation inducing a change of the CV shape, which then displayed the well-described oxidation wave of $H_2O_2$ plus the reduction wave of $O_2$ (light blue line).

These results demonstrate that superoxide anion $O_2^{\bullet-}$ appears and accumulates in alkaline phosphate buffers along their exposure to CAPs, at sufficiently high concentrations to be efficiently detected by cyclic voltammetry (tens of micromolars typical sensitivity for this method). When comparing the current intensity (same analytical conditions) obtained from a chemically-prepared solution of superoxide at 400 µM (~20 nA amplitude measured at 0 V, dashed line) and the amplitude obtained from the plasma-treated solution (~10 nA), we estimate that after 35 minutes of plasma exposure, the steady-state $O_2^{\bullet-}$ concentration in solution was about 200 µM.

Moreover, results in Figure 3 (light blue curve) show that the direct detection of superoxide in physiological conditions may be difficult because of its disproportionation rate at pH 7.4 (equation (2)). Nevertheless, $O_2^{\bullet-}$ is produced from a continuous source, i.e. the CAP, therefore leading to a competition between production and clearance rates, at least its disproportionation. Consequently, if the kinetic of production is faster than the disproportionation rate, as a function of the species concentration, an accumulation of superoxide anion in solution should be possible, allowing its detection even at physiological pH. Demonstrating this point is the goal of the next study.

**Study at physiological pH**

The measurements were then conducted at pH 7.4 in PBS by cyclic voltammetry in the same range of potentials than before (between -0.2 V and +0.5 V vs. Ag/AgCl). Typical CVs detected along a plasma exposure are presented in Figure 4A. From the first minutes of plasma exposure, we observed variations of the CV shape and current amplitudes (Figures 4A). One can observe the appearance of two oxidation waves (plateaus at about 0 V and +0.35 V vs. Ag/AgCl) and one reduction wave (plateau at about -0.15 V vs. Ag/AgCl), suggesting the presence of at least 3 redox species in the exposed solution. The oxidation wave observed between +0.05 V and +0.35 V vs. Ag/AgCl (Figure 4A), corresponds to the characteristic $H_2O_2$ oxidation signal on black-Pt modified UMEs.[29] The reductive wave between 0V and -0.2 V is likely attributed to $O_2$ and to $H_2O_2$, both species being reduced at similar potentials with black-Pt UMEs.[48] $O_2$ is naturally solubilized in solution (~220 µM concentration in aerated aqueous solutions under standard conditions) and can also be produced by side-decomposition reactions, including superoxide disproportionation.[48] As reported on Figure 4B, the current intensity measured at +0.35 V (dots), i.e. the plateau potential of $H_2O_2$ wave, increases over time, whereas the variations are not monotonic at the two other plateau potentials: at 0 V (triangles), the current slowly decreases for 25 min and then slightly increases for the rest of the plasma exposure duration, until reaching positive values of few nanoamperes after 40 minutes; at -0.2 V, the reductive current is stable for 20 min (Figure 4B, squares) and then increases (in absolute value). These variations of current intensity during the solution exposure to plasma indicate the formation and accumulation of the species in solution with different dynamics. A latency of ~20 min is observed at 0 V and -0.2 V to observe current variations, corresponding to the time necessary for species to accumulate enough to reach a concentration higher than the detection limit of the method, i.e. tens of micromolars with cyclic voltammetry at UMEs. The low positive oxidative current detected at 0 V is most likely due to the superoxide anion because the wave appearing in this potential range is perfectly similar to the one recorded in a superoxide anion solution (chemical origin), as shown in Figure 3. However, one should also consider that the baseline current at this potential is negative when hydrogen peroxide is simultaneously detected. Indeed, as illustrated in Figure S2 and in agreement with our previous works, platinum oxides (PtOx including $PtO_2$, PtO and PtOH) are formed in such conditions and are involved in the interaction with $H_2O_2$ during the electrochemical process.[49] Consequently, a reductive current should be detected at 0 V vs Ag/AgCl in a solution containing $H_2O_2$. This explains why the current at 0 V reported in Figure 4B first decreases when $H_2O_2$ is detected, and further increases due to the accumulation of another species, supposedly superoxide anion.

In order to confirm this hypothesis, we monitored the current evolution at 0 V over several minutes after the plasma was stopped. Superoxide is unstable at physiological pH, and if the species was not supplied anymore by the CAP, we should observe modifications in the CVs and a drop of current at neutral potential.

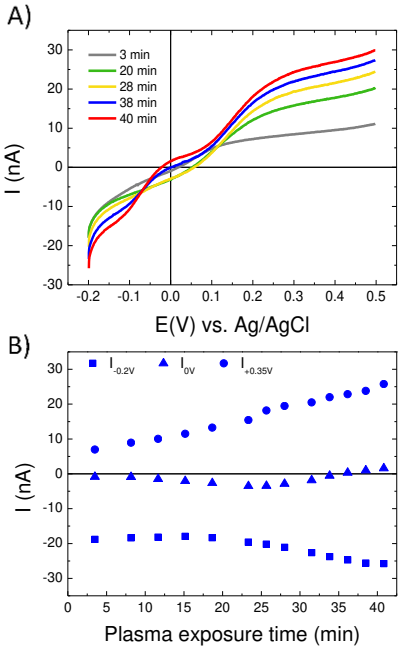


**Figure 4.** (A) Cyclic voltammograms recorded during the plasma exposure of a PBS solution (pH 7.4, 10 mM) with 100% $N_2$ as shielding gas. (B) Current values at -0.2 V (squares), 0 V (triangles) and +0.35 V vs. Ag/AgCl (dots) were extracted from the CV curves (in A) and plotted as a function of the plasma exposure time. CVs are measured between -0.2 V and +0.5 V vs. Ag/AgCl under constant magnetic stirring of the solution. Scan rate 20 $mV.s^{-1}$.

Corresponding results are shown on Figure 5A where we compared the CV cycle recorded after ~40 min of plasma exposure (blue line) with the cycle obtained after switching the plasma OFF and stabilization of the signal (~10 min, orange line). When the plasma was turned OFF, the oxidative and reductive currents corresponding to $H_2O_2$ and $O_2$ waves increased in amplitude, while the oxidative current near 0 V disappeared. This suggests first that the species oxidized near 0 V is indeed unstable, and second that the decomposition of the assumed superoxide anion is accompanied by the production of $H_2O_2$ and $O_2$. Considering previous data in alkaline condition, the electrochemical signature and kinetic evolutions of the signals, we conclude that the redox species leading to the additional current detected at 0 V in physiological conditions is superoxide anion. Its signal is even better observed when the baseline current (non-exposed PBS) is subtracted from the CV recorded under plasma exposure (Figure 5B). A reversible system at low potentials (between -0.2 and +0.05 V vs. Ag/AgCl) is observed, corresponding to the redox wave of superoxide anion detected in stable alkaline PBS (Figure 3). The reversible wave amplitude corresponded to about 50 µM of superoxide anion detected at steady-state produced by the CAP. Besides, no other redox RONS was reported to be detected at such low potential, near 0 V vs Ag/AgCl, on platinum electrodes. The formal redox potential E°' of the couple $O_2/O_2^{\bullet-}$ is indeed very low, i.e. -0.18 V vs RHE (pH 7.4). Further, an oxidation wave between +0.05 and +0.4 V vs. Ag/AgCl is observed, corresponding to the detection of $H_2O_2$ produced by the plasma and superoxide disproportionation.

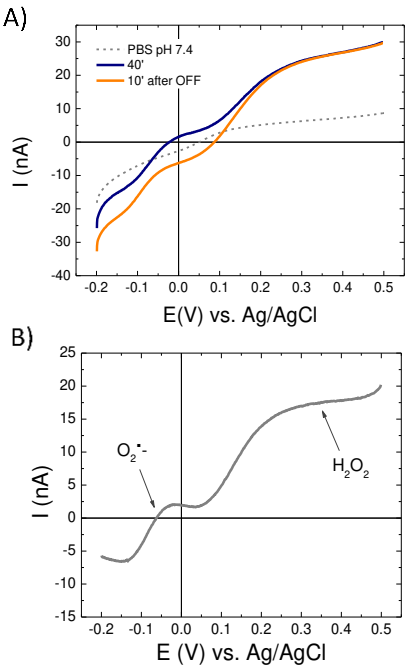


**Figure 5.** (A) Evolution of the voltammograms detected in a PBS solution before plasma exposure (dashed grey line), at the end of the plasma treatment, i.e. after 40 minutes of plasma exposure (blue line), and 10 minutes after the plasma was turned OFF (orange line), for 100% $N_2$ as shielding gas. CVs are measured between -0.2 V and +0.5 V under constant stirring of the solution. Scan rate 20 $mV.s^{-1}$. (B) Subtraction of the CV obtained after 40 min of plasma exposure from the baseline signal of the non-treated PBS.

This whole set of results demonstrate that superoxide is present in physiological PBS (pH 7.4) during its exposure to the plasma, first for a 100 % $N_2$ shielding gas condition. It means that, as long as the plasma is ON and after a certain time necessary for the species accumulation (~20-25 min in our experiments for 6 mL PBS volume), the superoxide concentration reaches a steady-state and sufficiently high level to be detected by cyclic voltammetry. As soon as the plasma is OFF, superoxide content rapidly vanishes (loss of current under few minutes, see Figure 6) to produce additional amounts of $H_2O_2$ and $O_2$.

**Correlations between plasma and liquid compositions**

The next challenge was to establish precise correlations between the composition of the plasma phase, controlled by the shielding gas composition, and the production of superoxide and other RONS in the liquid phase. Cyclic voltammetry measurements were performed in CAP-exposed PBS for each shielding gas composition (100 % $N_2$, 80 % $N_2$-20 % $O_2$ and 100 % $O_2$). In Figure 6A, CVs depict for both conditions of 100 % $N_2$ (blue line) and for 80 % $N_2$-20 % $O_2$ (green line) two oxidative waves that were attributed to superoxide (plateau current at 0 V) and $H_2O_2$ (plateau at +0.35 V). At 0 V, the current is higher for 80 % $N_2$-20 % $O_2$, than for 100 % $N_2$, whereas for 100 % $O_2$ (red line), only the oxidative wave corresponding to $H_2O_2$ is clearly observed. We can assume that superoxide generation is thus higher for 80 % $N_2$-20 % $O_2$ and 100 % $N_2$ than for 100 % $O_2$. After plasma was switched OFF (Figure 6B), the positive current at 0 V (noted $I_{0\,V}$) disappeared for both 100 % $N_2$ and 80 % $N_2$-20 % $O_2$, whereas the signal remained unchanged for 100 % $O_2$. In addition, the amperometric current $I_{0\,V}$ and the variation $I_{(+0.35\,V)} - I_{(+0.05\,V)}$ corresponding to $O_2^{\bullet-}$ and $H_2O_2$ intensities, respectively, were plotted as a function of time, for each shielding gas composition (Figures 6C and 6D). The current evolutions depict different phenomena:

1/ $I_{0\,V}$ decreases slightly over the first 30 minutes, because of the initial formation of PtOx along CVs of $H_2O_2$ solutions in this potential range (Figure S2). Though this process is complex, it is fully reproducible and was previously understood in the context of hydrogen peroxide detection with Black-Pt electrodes.[49] If $H_2O_2$ was alone in solution, the current $I_{0\,V}$ should only decrease (-10 nA maximum, corresponding to the reduction of formed PtOx). Instead, after t = 30 min of plasma exposure, $I_{0\,V}$ value increases progressively and becomes positive meaning that there is a latency phase necessary for the production and accumulation of superoxide in solution. The steady-state concentration of free superoxide becomes sufficiently high for the species to be detected by CV. Meanwhile, $H_2O_2$ accumulates in solution from t = 0, as shown in Figure 6D. Each shielding gas composition depicts a difference of signal during the latency period. This is correlated with kinetic variations of $H_2O_2$ generation (Figure 6D). $H_2O_2$ wave intensity increases faster for 100 % $N_2$ and 80 % $N_2$-20 % $O_2$ shieldings and slower for 100 % $O_2$.

2/ For the "air composition" shielding gas, $I_{0\,V}$ starts to increase slightly earlier than for 100 % $N_2$ (at ~20 and ~25 min, respectively) but both signals reach positive currents before plasma is switched OFF. This is associated with a stabilization of the current related to $H_2O_2$ for both 100 % $N_2$ and 80 % $N_2$-20 % $O_2$ (Figure 6D). Although the final $I_{0\,V}$ current value for the 80 % $N_2$-20 % $O_2$ shielding is higher than for 100 % $N_2$, a current variation of +6 nA was measured for both compositions. The discrepancy between maximal current values is simply due to a difference of the minimal current values originating from the faster kinetic of $H_2O_2$ production with the 100 % $N_2$ shielding, as shown on Figure 6D. For 100 % $O_2$, the current does not increase after the latency phase but we do observe a change of slope, which gets slower after ~30 min of plasma exposure. Even though this is less clear than for the other shielding gas composition, there is an effect of the plasma exposure on $I_{0\,V}$ for 100 % $O_2$, suggesting a small production of superoxide. In conclusion, in the first minutes, $H_2O_2$ appearance prevails over the one of superoxide, not concentrated enough to be observed. Then, $O_2^{\bullet-}$ concentration becomes sufficiently high to give a signal in CV that adds up to the $H_2O_2$ signal, inducing an overall increase of the current at 0 V.

3/ When the plasma exposure is turned OFF, $I_{0\,V}$ decreases for each condition (Figure 6C). This is consistent with the decomposition of $O_2^{\bullet-}$ in physiological conditions, leading to the decay of $I_{0\,V}$. We observe that the final value for $I_{0\,V}$ is lower than the initial level due to a higher concentration of $H_2O_2$ in solution, generated by the plasma and to the further superoxide disproportionation after plasma is turned OFF. Indeed, after plasma stopping, the current due to $H_2O_2$ still increases for each condition because of ensuing chemical reactions in solution. It becomes thus even clearer that superoxide is also generated for 100% $O_2$, as previously assumed. All these results provide direct and indirect proofs of superoxide anion existence and transient accumulation when CAPs interact with PBS and further, such interaction additionally depends on the environmental conditions. Furthermore, we observe that this chemistry leads to the formation of long-lived RONS such as $H_2O_2$ but also nitrate and nitrite.

**Study in physiological conditions of nitrite production**

Then, additional cyclic voltammetry experiments were

performed to monitor the formation of $NO_2^-$ during the plasma exposure. Nitrite are common chemical markers of the interaction of CAPs with aqueous solutions, usually the most concentrated stable species dissolved *in vitro* (nitrate as well, but they cannot be oxidized electrochemically). The range of scanned potentials in CV was extended to higher values in order to oxidize $NO_2^-$ on the platinized UMEs. Results are presented on Figure S3A, at an exposure time leading to observable waves and as function of the CAPs shielding gas. We observed that after ~30 minutes of plasma exposure, CVs depict 3 distinct responses (Figure S3A):

1/ Between +0.05 V and +0.35 V, the oxidation wave attributed to $H_2O_2$ is clearly observed and increase as function of time.

2/ Between +0.65 V and +0.85 V, an oxidative wave is visible for each condition, corresponding to $NO_2^-$ oxidation.

3/ Around 0 V, an oxidative current is again observed, only for 100 % $N_2$ and 80 % $N_2$-20 % $O_2$ conditions (blue and green lines, respectively), which is due to superoxide.

When the plasma was switched OFF, CVs were still recorded until a stable signal was reached (~10 min, Figure S3B). $H_2O_2$ and $NO_2^-$ oxidation waves reached constant amplitudes, whereas the oxidation wave observed at 0 V, attributed to superoxide anion, faded.

The fate of $H_2O_2$ and $NO_2^-$ as a function of time was further studied (Figure S5) by measuring the current differences corresponding to each oxidation wave, respectively $\Delta I_{H_2O_2} = I_{+0.35\,V} - I_{+0.05\,V}$ and $\Delta I_{NO_2^-} = I_{+0.85\,V} - I_{+0.65\,V}$ (Figures S5A and S5B). The *in situ* concentrations of $H_2O_2$ and $NO_2^-$ were calculated based on calibration curves obtained with the same electrodes (Figure S4).[29] We first observed that both species concentration depends on the shielding gas composition. Secondly, the kinetic evolution is different before and after the plasma is OFF, regardless of the shielding condition. On Figure S5A, the current due to $H_2O_2$ increases progressively for each condition. Higher values are reached under 100 % $N_2$ condition and a quasi-plateau level is observed after 20 min, as already observed in Figure 6D.

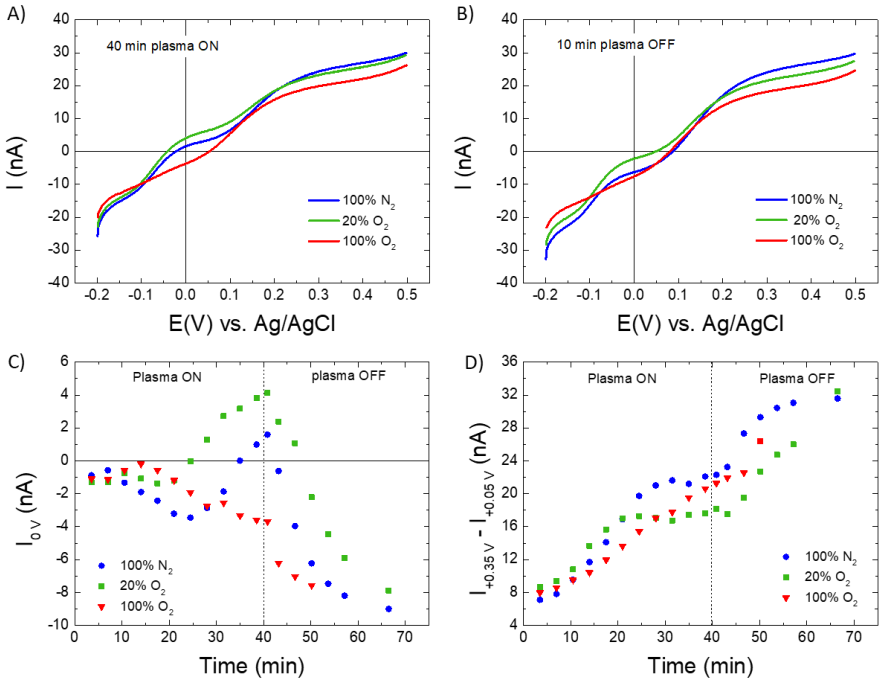


**Figure 6.** Cyclic voltammograms measured with platinized UMEs in PBS solution (pH 7.4): (A) during plasma exposure after 40 minutes of treatment; (B) 10 minutes after plasma was turned OFF. CVs were measured between -0.2 V and +0.5 V under magnetic stirring of the solution, for three conditions of the plasma shielding gas, i.e. 100% $N_2$ (blue line), 80% $N_2$/20% $O_2$ (green line) and 100% $O_2$ (red line). Scan rate 20 mV.s$^{-1}$. Current intensities are measured at 0 V (C) and I(+0.35 V) – I(+0.05 V) (D) and plotted as a function of time, to monitor superoxide and hydrogen peroxide dynamics, respectively, for each condition of shielding gas i.e. 100% $N_2$ (blue circles), 80% $N_2$/20% $O_2$ (green squares) and 100% $O_2$ (red triangles) and extracted from CV experiments

This shows that the accumulation of $H_2O_2$ does not only depend on its dissolution from the plasma phase, but as well on the disproportionation of superoxide which kinetic depends on its concentration, the local pH and the competition with other side reactions, e.g. the formation of peroxynitrite (reaction 4). As discussed earlier, superoxide disproportionation into $H_2O_2$ and $O_2$ continues after plasma is OFF, until all $O_2^{\bullet-}$ species are consumed, leading to a subsequent current rise. On Figure S5B, the current related to $NO_2^-$ increases linearly under plasma exposure and stabilizes just after plasma is turned OFF. Differently from $H_2O_2$, $NO_2^-$ is accumulating in solution progressively because this species (similarly for $NO_3^-$) originates from the dissolution of $HNO_2$ (and $HNO_3$, respectively) without any further side reactions. As a consequence, the nitrite concentration remains constant after stopping the plasma exposure. The shielding gas composition induces clear differences on the *in vitro* chemistry induced by CAPs. $H_2O_2$ and $NO_2^-$ concentrations reached after stabilization were plotted for each shielding gas condition (Figure S5C). As previously observed, $H_2O_2$ concentration is higher for 100 % $N_2$, i.e. 650 µM, while it reaches 550 µM for 80 % $N_2$-20 % $O_2$ and 420 µM for 100 % $O_2$. These results are consistent with the variations observed for $HO^\bullet$ in the gas phase (see Figure 2A): it reinforces the assessment that $HO^\bullet$ is one of the major gaseous mother species leading to $H_2O_2$ in plasma-treated PBS solution, according to the following equation:[50–52]

$$HO^\bullet + HO^\bullet + M \rightarrow H_2O_2 \qquad (8)$$

With M being a third collision partner in the gas phase. Hydrogen peroxide thus produced in the gas phase can be solvated into the liquid phase (high Henry's law constant).[50–53] It accumulates over time following this route, in addition to the superoxide disproportionation route explained before.[48]
The concentration of nitrite ions is slightly higher for 80 % $N_2$-20 % $O_2$ (670 µM) than for 100 % $N_2$ (650 µM), while it reaches only 300 µM for 100 % $O_2$. As previously described, $NO_2^-$ is expected to come from $HNO_2$ (nitrous acid) produced in the gas phase according to the following equation:[50,51,53]

$$HO^\bullet + NO^\bullet + M \rightarrow HNO_2 \quad (9)$$

Unfortunately, we did not detect by OES of the gas phase significant amounts $NO^\bullet$ in the current conditions. However, we observed in a previous study that $NO^\bullet$ emissive intensity strongly decreases when oxygen is added to the shielding gas.[19] The shielding gas effect is probably diminished herein because of the air-plasma interaction existing between the end of the tube and the liquid surface (open cell configuration). As a result, 100 % $N_2$ and the air-like condition, 80 % $N_2$-20 % $O_2$, should give close $NO^\bullet$ and therefore close $NO_2^-$ concentrations, which is in good agreement with our results. Similarly, 100 % $O_2$ should lead to a lower concentration of $NO_2^-$ (300 µM) such like we measured. Plasma-air interactions allow nitrogen to mix with the ionization wave and give rise to different gaseous nitrogen excited species detected by OES for the 100% $O_2$ condition (see Figures 2B and 2C). Moreover, we demonstrated previously that $NO_2^-$ accumulation is associated with pH variations of the PBS solution (10 mM), because of $HNO_2$ and $HNO_3$ acids dissolving from the gas phase.[36] Thus, we measured the pH evolution in plasma-treated solutions over 20 hours (data not shown). The results indicated that for 100 % $N_2$ and 80 % $N_2$-20 % $O_2$ the pH decreased by 0.25 unit from the initial value of 7.4. For 100 % $O_2$ the pH variation lowered of 0.17 pH unit. These variations are perfectly correlated with the detected $NO_2^-$ concentrations, which are higher for 100 % $N_2$ and 80 % $N_2$-20 % $O_2$. After plasma was stopped, the pH of the solutions did not vary significantly over time, meaning that reactions involving $HNO_2$ or other acidic species had reached their steady-state. In addition, we demonstrated previously the presence in solution of peroxynitrite anions ($ONOO^-$) produced according to equation (4).[19] In addition to the potent presence of $NO^\bullet$ in the gas phase and its dissolution in PBS, $O_2^{\bullet-}$ is present in solution and can thus react with $NO^\bullet$ (i.e. superoxide may consume all the available nitric oxide) to form $ONOO^-$.
Finally, the current results allow to propose a reaction scheme (scheme 1), which gives a non-exhaustive overview of the species and chemical reactions occurring in both the gas and liquid phases in our experimental conditions. Species that have been effectively detected and quantified in solution by combined electrochemistry and spectroscopic methods are highlighted by squares, some other species may be present (e.g. ozone, peroxynitrate, hypochlorite, chloramine, etc.) since they have been reported elsewhere and could be involved in cross-reactions.[32] All processes lead to the accumulation of certain RONS, in particular $O_2^{\bullet-}$, at concentrations being harmful for biological structures and entities.

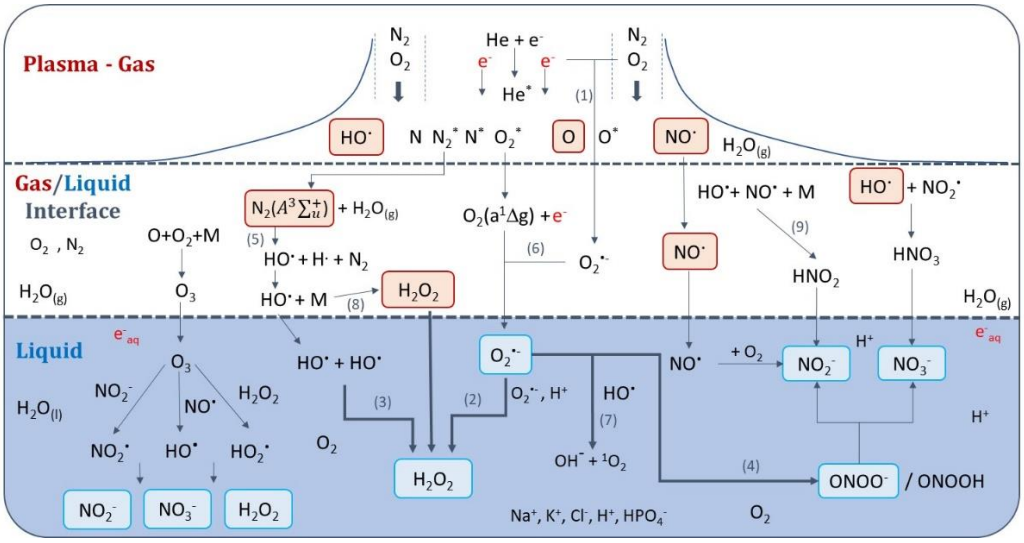


**Scheme 1.** Main chemical pathways of RONS formation in both plasma-gas and liquid phases. The major gaseous and liquid RONS detected in our studies are framed in blue. Equation numbers in the scheme correspond to the chemical equations described in the main text.

## CONCLUSION

We characterized the production of RONS in PBS during its exposure to cold atmospheric plasmas, and correlated the chemistry in solution with the nature of the gaseous environment surrounding the ionization waves. Electrically-shielded electrochemical sensors (UMEs), protected from the high voltage source of the plasma, provided *in situ* electrochemical measurements of superoxide anion, a redox ROS whose production by CAPs in solution was often hypothesized but never directly identified and quantified. Superoxide anion was successfully detected at micromolar concentrations (50 µM at most) in CAP exposed-phosphate buffers at both alkaline and physiological pH (pH 11 and 7.4). We detected the highest concentrations of RONS (including $H_2O_2$, $NO_2^-$ and $O_2^{\bullet-}$) when nitrogen is introduced in majority in the shielding gas (100 % $N_2$ and 80 % $N_2$-20 % $O_2$), while RONS production was strongly limited for 100 % $O_2$ in the shielding gas. Moreover, $O_2^{\bullet-}$ appears to be another major source of $H_2O_2$ in CAP-exposed PBS at pH 7.4 aside from the gas phase reaction that involves hydroxyl radicals. The *in situ*

monitoring of RONS generation should raise much interest for diverse applications of CAPs since real-time information is gained. It would be highly valuable to establish a spatial mapping of RONS generation during plasma treatments of living cells in culture and *in vivo* (e.g. skin cells). This will require a down-scaling of the electrochemical cell, in order to get closer to the plasma impact point without damaging its measurement ability.

## AUTHOR INFORMATION


### Corresponding Author

Dr Stéphane Arbault, email : stephane.arbault@u-bordeaux.fr, Tel.: +33540006851 ; Dr Franck Clément, email : franck.clement@univ-pau.fr, Tel.: +33559574190.


### Author Contributions

The manuscript was written through contributions of all authors. All authors have given approval to the final version of the manuscript.


### Present addresses

Current affiliations of F. Girard-Sahun, V. Badets are respectively: Chemistry Department, University of Antwerp, Campus Drie Eiken Universiteitsplein 1, Belgium. University of Strasbourg, Chemistry Institute, UMR CNRS 7177, 4 rue Blaise Pascal, CS 90032, 67081 Strasbourg Cedex, France.


## ACKNOWLEDGMENT


This work was financially supported by the Centre National de la Recherche Scientifique (CNRS), the French Ministry of Research (MESRI) and the Agence Nationale de la Recherche (ANR, PLASMAREGEN project, no. ANR-14-CE16-0007-01).


### Supporting Information

The Supporting Information is available free of charge on the ACS Publications website. 1) Optical emissive spectroscopy spectra of the gas phase for various shielding gas compositions; 2) Cyclic voltammetry in $H_2O_2$ (0.2 to 1 mM) and of 3)1 mM $H_2O_2$ + 1 mM $NO_2^-$ solutions prepared in PBS pH 7.4; 4) Cyclic voltammograms measured in PBS pH 7.4 after 30 min. plasma exposure and 10 min. after stop; 5) Measurements of the current variations and concentrations of $H_2O_2$ and $NO_2^-$ produced in PBS pH 7.4 by the 3 gas shielded plasmas.

## REFERENCES


(1) Graves, D. B. *Phys. Plasmas* **2014**, *21* (8), 080901.
(2) Lu, X.; Naidis, G. V.; Laroussi, M.; Reuter, S.; Graves, D. B.; Ostrikov, K. *Phys. Rep.* **2016**, *630*, 1–84.
(3) Privat-Maldonado, A.; Schmidt, A.; Lin, A.; Weltmann, K.-D.; Wende, K.; Bogaerts, A.; Bekeschus, S. *Oxid. Med. Cell. Longev.* **2019**, 1–29.
(4) Bauer, G. *Redox Biol.* **2019**, *26*, 101291.
(5) Bauer, G.; Sersenová, D.; Graves, D. B.; Machala, Z. *Sci. Rep.* **2019**, *9* (1), 13931.
(6) Bourdens, M.; Jeanson, Y.; Taurand, M.; Juin, N.; Carrière, A.; Clément, F.; Casteilla, L.; Bulteau, A.-L.; Planat-Bénard, V. *Sci. Rep.* **2019**, *9* (1), 8671.
(7) Arndt, S.; Schmidt, A.; Karrer, S.; von Woedtke, T. *Clin. Plasma Med.* **2018**, *9*, 24–33.
(8) Duchesne, C.; Frescaline, N.; Lataillade, J.-J.; Rousseau, A. *Plasma Med.* **2018**, *8(4)*, 379.
(9) Schmidt, A.; Niessner, F.; von Woedtke, T.; Bekeschus, S. *IEEE Trans. Radiat. Plasma Med. Sci.* **2020**, 5, 412-419.
(10) Lin, A.; Gorbanev, Y.; De Backer, J.; Van Loenhout, J.; Van Boxem, W.; Lemière, F.; Cos, P.; Dewilde, S.; Smits, E.; Bogaerts, A. *Adv. Sci.* **2019**, 1802062.
(11) Keidar, M. *Plasma Cancer Therapy*; Springer Series on Atomic, Optical, and Plasma Physics; Springer International Publishing, 2020; Vol. 115.
(12) Duday, D.; Clément, F.; Audinot, J.-N.; Belmonte, T.; Kutasi, K.; Cauchie, H.-M.; Choquet, P. *Plasma Process Polym* **2013**, *10*, 864-879.
(13) Machala, Z.; Tarabová, B.; Sersenová, D.; Janda, M.; Hensel, K. *J. Phys. Appl. Phys.* **2019**, *52* (3), 034002.
(14) Misra, N. N.; Yadav, B.; Roopesh, M. S.; Jo, C. *Compr. Rev. Food Sci. Food Saf.* **2019**, *18* (1), 106–120.
(15) Filipic, A.; Gutierrez-aguirre, I.; Primc, G.; Mozetic, M. *Trends Biotechnol.* **2020**, *38* (11), 1278–1291.
(16) Tresp, H.; Hammer, M. U.; Weltmann, K.-D.; Reuter, S. *Plasma Med.* **2013**, *3* (1–2), 45–55.
(17) Reuter, S.; Winter, J.; Iseni, S.; Schmidt-Bleker, A.; Dunnbier, M.; Masur, K.; Wende, K.; Weltmann, K.-D. *IEEE Trans. Plasma Sci.* **2015**, *43* (9), 3185–3192.
(18) Schmidt-Bleker, A.; Winter, J.; Bösel, A.; Reuter, S.; Weltmann, K.-D. *Plasma Sources Sci. Technol.* **2016**, *25* (1), 015005.
(19) Girard, F.; Peret, M.; Dumont, N.; Badets, V.; Blanc, S.; Gazeli, K.; Noël, C.; Belmonte, T.; Marlin, L.; Cambus, J.-P.; Simon, G.; Sojic, N.; Held, B.; Arbault, S.; Clément, F. *Phys. Chem. Chem. Phys.* **2018**, *20* (14), 9198–9210.
(20) Darny, T.; Pouvesle, J.-M.; Puech, V.; Douat, C.; Dozias, S.; Robert, E. *Plasma Sources Sci. Technol.* **2017**, *26* (4), 045008.
(21) Jõgi, I.; Talviste, R.; Raud, S.; Raud, J.; Plank, T.; Moravský, L.; Klas, M.; Matejčík, Š. *Contrib. Plasma Phys.* **2020**, *60* (3), e201900127.
(22) Gazeli, K.; Svarnas, P.; Lazarou, C.; Anastassiou, C.; Georghiou, G. E.; Papadopoulos, P. K.; Clément, F. *Phys. Plasmas* **2020**, *27* (12), 123503.
(23) Slikboer, E.; Acharya, K.; Sobota, A.; Garcia-Caurel, E.; Guaitella, O. *Sci. Rep.* **2020**, *10* (1), 2712.
(24) Babaeva, N. Yu.; Naidis, G. V. *J. Appl. Phys.* **2020**, *128* (20), 203301.
(25) Gorbanev, Y.; O'Connell, D.; Chechik, V. *Chem. - Eur. J.* **2016**, *22*, 3496–3505.
(26) Gorbanev, Y.; Privat-Maldonado, A.; Bogaerts, A. *Anal. Chem.* **2018**, *90* (22), 13151–13158.
(27) Gorbanev, Y.; Bogaerts, A. Chemical Detection of Short-Lived Species Induced in Aqueous Media by Atmospheric Pressure Plasma. In *Atmospheric Pressure Plasma*; Nikiforov, A., Chen, Z., Eds.; IntechOpen: Rijeka, 2019.
(28) Attri, P.; Kim, Y. H.; Park, D. H.; Park, J. H.; Hong, Y. J.; Uhm, H. S.; Kim, K.-N.; Fridman, A.; Choi, E. H. *Sci. Rep.* **2015**, *5* (1), 9332.
(29) Girard-Sahun, F.; Badets, V.; Lefrançois, P.; Sojic, N.; Clement, F.; Arbault, S. *Anal. Chem.* **2019**, *91* (13), 8002–8007.
(30) Goldberg, B. M.; Chng, T. L.; Dogariu, A.; Miles, R. B. *Appl. Phys. Lett.* **2018**, *112* (6), 064102.
(31) Sretenović, G. B.; Krstić, I. B.; Kovačević, V. V.; Obradović, B. M.; Kuraica, M. M. *Appl. Phys. Lett.* **2011**, *99* (16), 161502.
(32) Nasri, Z.; Bruno, G.; Bekeschus, S.; Weltmann, K.-D.; von Woedtke, T.; Wende, K. *Sens. Actuators B Chem.* **2021**, *326*, 129007.
(33) Hayyan, M.; Hashim, M. A.; AlNashef, I. M. *Chem. Rev.* **2016**, *116*, 3029–3085.
(34) Xu, D.; Liu, D.; Wang, B.; Chen, C.; Chen, Z.; Li, D.; Yang, Y.; Chen, H.; Kong, M. G. *PLOS ONE* **2015**, *10*, e0128205.
(35) Reuter, S. *Appl Phys* **2018**, *51*, 52.
(36) Girard, F.; Badets, V.; Blanc, S.; Gazeli, K.; Marlin, L.; Authier, L.; Svarnas, P.; Sojic, N.; Clément, F.; Arbault, S. *RSC Adv.* **2016**, *6* (82), 78457–78467.
(37) Gazeli, K.; Svarnas, P.; Held, B.; Marlin, L.; Clément, F. *J. Appl. Phys.* **2015**, *117*, 093302.
(38) Tresp, H.; Hammer, M. U.; Winter, J.; Weltmann, K.-D.; Reuter, S. *J. Phys. Appl. Phys.* **2013**, *46*, 435401.
(39) Cabrellon, G.; Tampieri, F.; Rossa, A.; Barbon, A.; Marotta, E.; Paradisi, C. *ACS Sens.* **2020**, *5*, 2866–2875.
(40) Chauvin, J.; Gibot, L.; Griseti, E.; Golzio, M.; Rols, M.-P.; Merbahi, N.; Vicendo, P. *Sci. Rep.* **2019**, *9*, 4866.

(41) Jablonowski, H.; Hänsch, M. A. Ch.; Dünnbier, M.; Wende, K.; Hammer, M. U.; Weltmann, K.-D.; Reuter, S.; von Woedtke, T. *Biointerphases* **2015**, *10*, 029506.
(42) Liu, Z.; Xu, D.; Liu, D.; Cui, Q.; Cai, H.; Li, Q.; Chen, H.; Kong, M. G. *J. Phys. Appl. Phys.* **2017**, *50*, 195204.
(43) Pouvesle, J.-M.; Darny, T.; Maho, T.; Puech, V.; Douat, C.; Dozias, S.; Robert, E. *Plasma Med.* **2018**, *8*, 83–92.
(44) Clément, F.; Held, B.; Soulem, N.; Guimon, C. *Eur Phys J AP* **2002**, *18*, 135–151.
(45) Jablonowski, H.; Santos Sousa, J.; Weltmann, K.-D.; Wende, K.; Reuter, S. *Sci. Rep.* **2018**, *8*, 12195.
(46) Ben-Amor, S.; Devin, A.; Rigoulet, M.; Sojic, N.; Arbault, S. *Electroanalysis* **2013**, *25*, 656–663.
(47) Ben-Amor, S.; Vanhove, E.; Sékli Belaïdi, F.; Charlot, S.; Colin, D.; Rigoulet, M.; Devin, A.; Sojic, N.; Launay, J.; Temple-Boyer, P.; Arbault, S. *Electrochimica Acta* **2014**, *126*, 171–178.
(48) Lefrançois, P.; Girard-Sahun, F.; Badets, V.; Clément, F.; Arbault, S. *Electroanalysis* **2021**, *33*, 882 –890.
(49) Badets, V.; Pandard, J.; Sojic, N.; Arbault, S. *ChemElectroChem* **2016**, *3* (12), 2288–2296.
(50) Bruggeman, P.; Schram, D. C. *Plasma Sources Sci. Technol.* **2010**, *19* (4), 045025.
(51) Sakiyama, Y.; Graves, D. B.; Chang, H.-W.; Shimizu, T.; Morfill, G. E. *J. Phys. Appl. Phys.* **2012**, *45* (42), 425201.
(52) Zhang, Z.; Xu, Z.; Cheng, C.; Wei, J.; Lan, Y.; Ni, G.; Sun, Q.; Qian, S.; Zhang, H.; Xia, W.; Shen, J.; Meng, Y.; Chu, P. K. *Plasma Chem. Plasma Process.* **2017**, *37* (2), 415–431.
(53) Tian, W.; Kushner, M. J. *J. Phys. Appl. Phys.* **2014**, *47* (16), 165201.

**Figure for Table of Contents Only**